Results in Applied Mathematics 4 (2019) 100081

Contents lists available at ScienceDirect

Results in Applied Mathematics

journal homepage: www.elsevier.com/locate/results-in-applied-mathematics

An a posteriori error analysis for a coupled continuum pipe-flow/Darcy model in Karst aquifers: Anisotropic and isotropic discretizations

Houédanou Koffi Wilfrid *

Université d'Abomey-Calavi (UAC), Republic of Benin
African Institute for Mathematical Sciences (AIMS), South Africa

ARTICLE INFO

Article history:
Received 22 July 2019
Received in revised form 15 October 2019
Accepted 20 October 2019
Available online 1 November 2019

MSC:
74S05
74S10
74S15
74S20
74S25
74S30

Keywords:
Karst aquifers
Anisotropic meshes
Error estimator

ABSTRACT

This paper presents an a posteriori error analysis for a coupled continuum pipe-flow/Darcy model in Karst aquifers. We consider a unified anisotropic finite element discretization (i.e. elements with very large aspect ratio). Our analysis covers two-dimensional domains, conforming and nonconforming discretizations as well as different elements. Many examples of finite elements that are covered by analysis are presented. From the finite element solution, the error estimators are constructed and based on the residual of model equations. Lower and upper error bounds form the main result with minimal assumptions on the elements. The lower error bound is uniform with respect to the mesh anisotropy in the entire domain. The upper error bound depends on a proper alignment of the anisotropy of the mesh which is a common feature of anisotropic error estimation. In the special case of isotropic meshes, the results simplify, and upper and lower error bounds hold unconditionally.

1. Introduction

A coupled continuum pipe-flow (CCPF) model has been developed for groundwater flow and solute transport in a Karst aquifer with conduits. Groundwater flow in conduits is simulated through pipe-flow model and flow in fissured matrix rock is described by Darcy's law. Water mass exchange between the two domains is modeled by a first-order exchange rate method. Karst aquifers are very vulnerable sources of groundwater which are largely used as drinkable and industrial water, especially as the aquifers are now being seriously threatened by increasing contamination. Therefore, it is practical for us to study the complicated systems like Karst aquifers for assessing groundwater risk and controlling groundwater pollution. One of the most popular models is so called coupled continuum pipe-flow/Darcy (CCPF) model in which the conduits embedded in the continuum matrix are simplified into a network of one-dimensional (1D) pipes [1–6].

Generally, the flow in the porous matrix is modeled by a continuum approach using the steady Boussinesq equation [7], and the Darcy–Weisbach equation [8] is applied to the conduit flow in the tube. The matrix flow and conduit flow are coupled at the intersection by the exchange flux, which is determined linearly by the difference of hydraulic heads between the matrix system and the conduit system, see [6,9–11].

* Correspondence to: Université d'Abomey-Calavi (UAC), Republic of Benin.
E-mail addresses: houedanou@aims.ac.za, khouedanou@yahoo.fr.

https://doi.org/10.1016/j.rinam.2019.100081

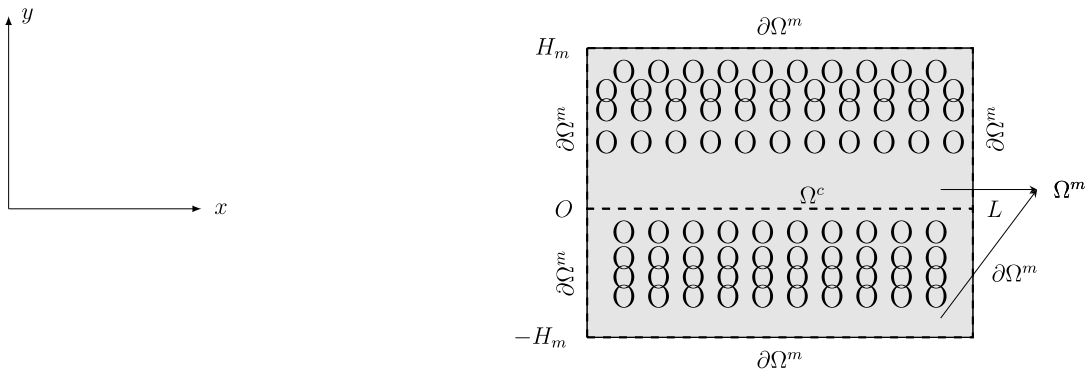

Fig. 1. Two-dimensional figure of a Karst aquifers.

Near the pipe-flow region (see Fig. 1), the derivative of the analytic solution in porous media on y-direction is with a low regularity. It means that the solution of Darcy model in the porous media domain varies significantly along the direction parallel to y-axis and is smooth along parallel to x-axis. Then it is better to use the anisotropic mesh with a small mesh size on the y-direction near pipe-line and a large mesh size elsewhere, which has the advantage of improving the computational accuracy and decreasing the amount of calculation comparing with refining grid in all directions. In [6,12–16], and in the references therein, we can find a large list of contributions devoted to numerically approximate the solution of this interaction problem, including conforming and nonconforming methods.

A posteriori error estimators are computable quantities, expressed in terms of the discrete solution and of the data that measure the actual discrete errors without the knowledge of the exact solution. They are essential to design adaptive mesh refinement algorithms which equi-distribute the computational effort and optimize the approximation efficiency. Since the pioneering work of Babuška and Rheinboldt [17], adaptive finite element methods based on a posteriori error estimates have been extensively investigated. To our best knowledge, there is no a posteriori error estimation for the CCPF/Darcy model valid for anisotropic and isotropic discretizations with finite element methods. Here, we develop such a posteriori error analysis for anisotropic finite elements satisfying minimal assumptions. These assumptions may be summarized as follows: the scheme is stable (not essential but recommended in numerical applications), the discrete space is large enough to contain the conforming $\mathbb{P}^1$ piecewise space and satisfies a Crouzeix–Raviart property (see below for the details). These three properties are satisfied by some standard finite elements like the Crouzeix–Raviart element, modified Crouzeix–Raviart elements [18] and the $\mathbb{Q}^k(k \geqslant 2)$ element on some anisotropic meshes.

The paper is organized as follows. Section 2 introduces the problem and some notation. The discretization (as discrete formulation) and the general framework with minimal conditions on the mesh and on the elements are given in Section 3. Section 4 is devoted to analytical tools. In Section 5 we present several examples of finite elements that are covered by our analysis. The actual error bounds are given in Section 6. For the upper error bound, we additionally distinguish between conforming and nonconforming discretization. While all these considerations are made for anisotropic meshes, we simplify the results for the case of an isotropic discretization in Section 6.4 since even in that case we obtain new results. We offer our conclusion and the further works in Section 7.

2. Preliminaries and notation

2.1. Model problem

For simplification, similarly to Cao et al. [6], we suppose the porous matrix domain $\Omega^m = \Omega^m_+ \cup \Omega^m_-$, with $\Omega^m_- =]0, L[\times] - H_m, 0[$ and $\Omega^m_+ =]0, L[\times[0, H_m[$; and the conduit pipe $\Omega^c =]0, L[\times\{y = 0\}$. $2H_m$ is the height of the matrix and L is the horizontal length of the matrix and conduit (see Fig. 1). We set $\Omega = \Omega^m \cup \Omega^c$. For each function v defined in Ω, because its restriction to Ω^m or to Ω^c could play a different Mathematical roles (for instance their traces on $]0, L[$), we will set $v^m = v_{|\Omega^m}$ and $v^c = v_{|\Omega^c}$. Thus, the two-dimensional (2D) steady-state CCPF/Darcy model in Karst aquifers can be written in the following form:

$$\begin{cases} -\operatorname{div}(\mathbb{K}\nabla u^m) &= -\alpha_{ex}(u^m - u^c)\delta_y + f^m & \text{in } \Omega^m \\ -\frac{d}{dx}\left(D\frac{du^c}{dx}\right) &= \alpha_{ex}\left(u^m{}_{|y=0} - u^c\right) + f^c & \text{in } \Omega^c, \end{cases} \tag{1}$$

with the Dirichlet boundary conditions,

$$\begin{cases} u^m = g^m & \text{on} \quad \partial\Omega^m, \\ u^c = g^c & \text{on} \quad \partial\Omega^c, \end{cases} \tag{2}$$

where u^m and u^c denote the unknown hydraulic heads in the porous matrix Ω^m and conduit pipe Ω^c, respectively. Under the homogeneous isotropic media assumption, the hydraulic conductivity tensor $\mathbb{K}$ takes the form $\mathbb{K} = \mathcal{K}\mathbb{I}$. Here, $\mathcal{K}$ is a constant, $\mathcal{K} = \frac{kg}{\mu}$, where k is the constant matrix permeability, μ the kinematic viscosity of water, and g the gravitational acceleration constant. The conductivity constant D depends on the width of the conduit d, $D = \frac{d^3 g}{12\mu}$. f^m and f^c represent the external source or sink terms. δ_y is the Dirac delta function concentrated on the straight line $\{y = 0\}$. The nonnegative constant α_{ex} represents the coefficient of flux exchange at the intersection between the matrix and conduit flow. Physical experimental results in [19–22] show that the CCPF model is valid for flows in Karst aquifers when a suitable fluid exchange coefficient α_{ex} is taken. We also suppose the homogeneous boundary condition, $g^m = 0 = g^c$, which can be easily extended to a general nonhomogeneous case. The system (1)–(2) consists of an elliptic equation governing the Darcy flow in the porous matrix region Ω^m and an embedded one-dimensional pipe-flow equation in conduit region Ω^c.

2.2. Weak formulation

In this section we introduce a weak formulation for the coupled problem given by (1) to (2). We begin this subsection by introducing some useful notations. If W is an open bounded domain of $\mathbb{R}^2$ and r is a nonnegative integer, the Sobolev space $H^r(W) = W^{r,2}(W)$ is defined in the usual way with the usual norm $\|\cdot\|_{r,W}$ and semi-norm $|\cdot|_{r,W}$. In particular, $H^0(W) = L^2(W)$ and we write $\|\cdot\|_W$ for $\|\cdot\|_{0,W}$. Similarly we denote by $(\cdot,\cdot)_W$ the $L^2(W)$ inner product. For shortness if W is equal to $\Omega := \Omega^m \cup \Omega^c$, we will drop the index Ω, while for any $r \geq 0$, $\|\cdot\|_{r,*} = \|\cdot\|_{r,\Omega_*}$, $|\cdot|_{r,*} = |\cdot|_{r,\Omega_*}$ and $(.,.)_* = (\cdot,\cdot)_{\Omega_*}$, for $* \in \{m, c\}$. The space $H_0^r(W)$ denotes the closure of $C_0^\infty(W)$ in $H^r(W)$.

We define the Hilbert space

$$V := \left\{ v \in H_0^1(\Omega) : v = 0 \text{ on } \partial\Omega^c \right\},$$

with the norm

$$\|v\|_V := |v|_{1,m} + \|v\|_{1,c}, \ \forall v \in V. \tag{3}$$

Let us further introduce the bilinear form, $a : V \times V \longrightarrow \mathbb{R}$ define for $u, v \in V$ by:

$$a(u, v) := a_m(u, v) + a_c(u, v), \tag{4}$$

where,

$$a_m(u, v) := \int_{\Omega^m} \mathbb{K}\nabla u^m \cdot \nabla v^m(x, y)dxdy, \tag{5}$$

and

$$\begin{aligned} a_c(u, v) := & \int_0^L D\frac{du^c}{dx} \cdot \frac{dv^c}{dx}dx \\ & + \alpha_{ex} \int_0^L \left(u^m(x, 0) - u^c(x)\right) v^m(x, 0)dx \\ & - \alpha_{ex} \int_0^L \left(u^m(x, 0) - u^c(x)\right) v^c(x)dx. \end{aligned} \tag{6}$$

In addition, we define the linear form on V by

$$F(v) := (f^m, v^m)_m + (f^c, v^c)_c, \tag{7}$$

with $v = (v^m, v^c)$ and $f = (f^m, f^c)$.

The weak formulation of the simplified CCPF model (1)–(2) can be stated as follows: find $u \in V$ such that,

$$a(u, v) = F(v) \ \forall v \in V. \tag{8}$$

Indeed, the weak solution u of simplified CCPF model (1)–(2) exists and is unique. This is a straight application of Lax–Milgram theorem on the fact that the bilinear form $a(u, v)$ on $V \times V$ satisfies the continuity and coercivity conditions.

In summary the following results hold:

Theorem 2.1. *If $f^* \in L^2(\Omega^*)$ for $* \in \{m, c\}$, then there exists a unique solution $u \in V$ to the problem (8).*

Remark 2.1. We remark that the form a_m is $|\cdot|_{1,\Omega^m}$-coercive on $H_0^1(\Omega^m)$ and the form a_c is $\|\cdot\|_{1,\Omega^c}$-coercive on $H_0^1(\Omega^c)$. Namely, there exist two constants $c_1 > 0$, $c_2 > 0$ such that:

$$a_m(v^m, v^m) \geq c_1|v^m|_{1,m}^2, \forall v^m \in H_0^1(\Omega^m), \tag{9}$$

and

$$a_c(v^c, v^c) \geq c_2\|v^c\|_{1,c}^2, \forall v^c \in H_0^1(\Omega^c). \tag{10}$$

We end this section with some notation. Let $\mathbb{P}^k$ and $\mathbb{Q}^k$ be the space of polynomials of total and partial degree not larger than k, respectively. In order to avoid excessive use of constants, the abbreviations $x \lesssim y$ and $x \sim y$ stand for $x \leqslant cy$ and $c_1 x \leqslant y \leqslant c_2 x$, respectively, with positive constants independent of x, y or $\mathcal{T}_h$ (meshes).

3. Anisotropic finite element method for CCPF/Darcy model

The first two sections introduce general aspects of the discretization, e.g; the finite element formulation. Section 3.3 is then devoted to the introduction of anisotropic quantities. The general framework (mesh and general assumptions) will be discussed in Section 3.5. As it turns out, the assumptions introduced on the mesh for anisotropic elements are quite weak, standard in anisotropic a posteriori error analysis and similar to the one for isotropic elements.

3.1. Discretization of the domain Ω

Since the existence of Dirac delta function, the analytic solution u^m of (1) may have anisotropic behavior near the straight line $\{y = 0\}$. Then, we consider to use anisotropic mesh with a small mesh size on y-direction near the line $\{y = 0\}$ and a larger mesh size elsewhere.

We now let $\mathcal{T}_h^+$ and $\mathcal{T}_h^-$ be members of families of triangulations of $\overline{\Omega_+^m}$ and $\overline{\Omega_-^m}$, respectively, by triangles or rectangles K of diameter h_K, and we assume that the vertices of $\mathcal{T}_h^+$ and $\mathcal{T}_h^-$ coincide on the interface $[0, L]$. Also, we let $h := \max\{h_-, h_+\}$, where $h_s := \max\{h_K : K \in \mathcal{T}_h^s\}$ for each $s \in \{+, -\}$. Thereby, let E_h be the corresponding induced triangulations of $\overline{\Omega^c}$. Noted that according to this discretization, E_h is not necessarily regular. Finally $\mathcal{T}_h = \mathcal{T}_h^+ \cup \mathcal{T}_h^-$ is the triangulation on $\overline{\Omega}$.

For any $K \in \mathcal{T}_h$, we denote by $\mathcal{E}(K)$ (resp. $\mathcal{N}(K)$) the set of its edges (resp. vertices) and we set $\mathcal{E}_h = \bigcup_{K\in\mathcal{T}_h} \mathcal{E}(K)$, $\mathcal{N}_h = \bigcup_{K\in\mathcal{T}_h} \mathcal{N}(K)$. For $\mathcal{A} \subset \overline{\Omega}$ we define

$$\mathcal{E}_h(\mathcal{A}) := \{E \in \mathcal{E}_h : E \subset \mathcal{A}\} \text{ and } \mathcal{N}_h(\mathcal{A}) := \{\mathbf{x} \in \mathcal{N}_h : \mathbf{x} \in \mathcal{A}\}.$$

The measure of an element or edge is denoted by $|K| := \text{meas}_i(K)$ and $|E| := \text{meas}_{i-1}(E)$, respectively, where $i = 2$.

For an edge E of a element K introduce the outer normal vector by $\mathbf{n} = (n_x, n_y)^\top$. Furthermore, for each segment E we fix one of the two normal vectors and denote it by $\mathbf{n}_E$. We introduce additionally the tangent vector $\mathbf{t} = \mathbf{n}^\top := (-n_y, n_x)^\top$ such that it is oriented positively (with respect to K). Similarly set $\mathbf{t}_E := \mathbf{n}_E^\top$. The superscript $\top$ denotes transposition. For any $E \in \mathcal{E}_h$ and any piecewise continuous function φ, we denote by $[\varphi]_E$ its jump across E in the direction of $\mathbf{n}_E$:

$$[\varphi]_E(x) := \begin{cases} \lim\limits_{t\to 0+} \varphi(x + t\mathbf{n}_E) - \lim\limits_{t\to 0+} \varphi(x - t\mathbf{n}_E) & \text{for an interior edge/face } E, \\ -\lim\limits_{t\to 0+} \varphi(x - t\mathbf{n}_E) & \text{for a boundary edge/face } E. \end{cases}$$

Note that the sign of $[\varphi]_E$ depends on the orientation of $\mathbf{n}_E$. However, terms such as a gradient jump $[\nabla\varphi \cdot \mathbf{n}_E]_E$ are independent of this orientation.

Furthermore one requires local subdomains (also known as patches). As usual, let W_K be the union of all elements having a common face with K. Similarly let W_E be the union of both elements having E as face (with appropriate modifications for a boundary face). By $W_{\mathbf{x}}$ we denote the union of all elements having $\mathbf{x}$ as node.

Later on we specify additional, mild mesh assumptions that are partially due to the anisotropic discretization.

3.2. Discrete formulation

We apply the finite element based on the anisotropic mesh $\mathcal{T}_h$ to solve the CCPF model (1)–(2). We assume a given approximation space V_h made of polynomials on each element K of the triangulation $\mathcal{T}_h$ such that $V_h^c \subset H_0^1(\Omega^c)$ (but not necessary $V_h^m \subset H_0^1(\Omega^m)$), where $V_h^* = \{v_{|\Omega^*} : v \in V_h\}$ for each $* \in \{m, c\}$. A precise description of the properties that this approximation space V_h has to satisfy is given in Section 3.5.

Because the approximation space V_h^m may not be included in the continuous space $H_0^1(\Omega^m)$, we define the approximation solution by using the weaker bilinear form $a_h(.,.)$:

$$\begin{aligned} a_h(u, v) := & \sum_{K\in\mathcal{T}_h} \mathbb{K}\nabla u^m \cdot \nabla v^m(x, y)dxdy \\ & + \int_0^L D\frac{du^c}{dx} \cdot \frac{dv^c}{dx}dx \\ & + \alpha_{ex} \int_0^L \left(u^m(x, 0) - u^c(x)\right) v^m(x, 0)dx \\ & - \alpha_{ex} \int_0^L \left(u^m(x, 0) - u^c(x)\right) v^c(x)dx. \end{aligned} \tag{11}$$

Fig. 2. Notation of rectangle K.

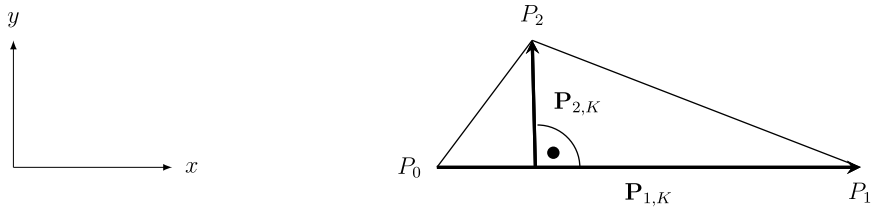

Fig. 3. Notation of triangle K.

Then, the finite element discretization of (8) is to find $u_h \in V_h$ such that

$$a_h(u_h, v_h) + J(u_h, v_h) = F(v_h)\ \forall v_h \in V_h. \tag{12}$$

This is the natural discretization of the weak formulation (8) except that the penalizing term $J(u_h, v_h)$ is added (only nonconforming case). These penalizing term will be specified later in the Section 5. The space V_h is equipped with the norm $\|\cdot\|_h := \|\cdot\|_V$ if $V_h \subset V$ whereas the norm $\|\cdot\|_h$ on V_h will be specified later in Section 5 for non-conforming case.

3.3. Anisotropic quantities

For an element $K \in \mathcal{T}_h$ we define two anisotropy vectors $\mathbf{P}_{i,K}$, $i = 1, 2$, that reflect the main anisotropy directions of that element. These anisotropy vectors are defined and visualized below as well (Figs. 2 and 3). The anisotropy vectors $\mathbf{P}_{i,K}$ are enumerated such that lengths are decreasing, i.e. $|\mathbf{P}_{1,K}| \geqslant |\mathbf{p}_{2,K}|$. The anisotropic lengths of an element K are now defined by $h_{j,K} := |\mathbf{P}_{j,K}|$, $(j = 1, 2)$ which implies $h_{1,K} \geq h_{2,K}$. The smallest of these lengths is particularly important; thus we introduce $h_{\min,K} := h_{2,K} \equiv \min_{i\in\{1,2\}} h_{i,K}$. Finally the anisotropy vectors $\mathbf{P}_{j,K}$ are arranged columnwise to define a matrix:

$$\mathbb{C}_K := [\mathbf{P}_{1,K}, \mathbf{P}_{2,K}] \in \mathbb{R}^{2,2}. \tag{13}$$

Note that $\mathbb{C}_K$ is orthogonal since anisotropy vectors $\mathbf{P}_{j,K}$ are also orthogonal and

$$\mathbb{C}_K^\top \cdot \mathbb{C}_K = \operatorname{diag}\{h_{1,K}^2, h_{2,K}^2\}. \tag{14}$$

Furthermore introduce the height $h_{E,K}$ over an edge E of an element K by

$$h_{E,K} := \frac{|K|}{|E|}. \tag{15}$$

Sometimes it is more convenient to have face-related data instead of element-related data. Hence for an interior face $E = K_1 \cap K_2$ we introduce

$$h_{\min,E} := \frac{h_{\min,K_1} + h_{\min,K_2}}{2} \text{ and } h_E := \frac{h_{E,K_1} + h_{E,K_2}}{2}.$$

For boundary faces $E \subset \partial K$ simply set $h_{\min,E} := h_{\min,K}$, $h_E := h_{E,K}$. The last assumption from below (Assumption 3.1) readily implies

$$h_E \sim h_{E,K_1} \sim h_{E,K_2} \text{ and } h_{\min,E} \sim h_{\min,K_1} \sim h_{\min,K_2}. \tag{16}$$

3.4. Relation between anisotropic mesh and anisotropic function

When investigating a residual error estimator for anisotropic meshes, we want to employ the same basic principles as for isotropic meshes. More precisely, a certain kind of interpolation error estimates is to be derived first. With its help, the finite element error is then bounded globally from above.

Proceeding this way, we naturally use different and more technical methods than for isotropic meshes. But even more important, the results of isotropic meshes cannot be transferred identically to anisotropic meshes. A certain factor appears now both at the interpolation error estimates (see Section 4.1) and the finite element error estimate (cf. Section 6). This factor is related to how good the chosen anisotropic mesh corresponds to the anisotropic function under consideration. Basically, the better this correspondence the smaller the factor (but always $\geqslant 1$), and the better the estimate (in a meaning that is to be specified later on). The importance of an anisotropic mesh that corresponds to an anisotropic function can be described and interpreted in different ways (Ref. [23, Page 33]).

We present now the definition of an alignment measure which measures the alignment of mesh and function.

Definition 3.1 (*Alignment Measure* m_1)**.** Let $v \in H^1(\Omega)$ be an arbitrary non-constant function. Define the matching function $m_1(.,.) : H^1(\Omega) \times \mathcal{T}_h \longrightarrow \mathbb{R}$ by [18,23,24]

$$m_1(v, \mathcal{T}_h) := \frac{\left(\sum_{K\in\mathcal{T}_h} h_{\min,K}^{-2} \|\mathbb{C}_K^\top \nabla v\|_K^2\right)^{1/2}}{\|\nabla v\|_\Omega}. \tag{17}$$

Commentary 3.1 (*Alignment Measure*)**.** For a better understanding we discuss here the behavior of the alignment measure. The structure of the matrix $\mathbb{C}_K$ from (13) readily gives the crude bounds,

$$1 \leqslant m_1(v, \mathcal{T}_h) \leqslant \max_{K\in\mathcal{T}_h} \frac{h_{\max,K}}{h_{\min,K}}, \tag{18}$$

where $h_{\max,K} \equiv h_{1,K}$ temporarily denotes the largest element dimension. Although this bound is practically useless, it implies an interesting by-product for isotropic meshes. There one concludes $m_1(v, \mathcal{T}_h) \sim 1$, and the alignment measure merges with other constants and thus "vanishes".

For anisotropic meshes, the term $\mathbb{C}_K^\top \nabla v$ of (17) contains directional derivatives along the main anisotropic directions $\mathbf{P}_{i,K}$ of the element K [since $\mathbb{C}_K = [\mathbf{P}_{1,K}, \mathbf{P}_{2,K}]$, see (13)]. Consider first anisotropic elements that are aligned with an anisotropic function v. Then the long anisotropic element direction $\mathbf{P}_{1,K}$ is associated with a small directional derivative $\mathbf{P}_{1,K}^\top \cdot \nabla v$. Conversely, the short direction $\mathbf{P}_{2,K}$ has a comparatively large directional derivative $\mathbf{P}_{2,K}^\top \cdot \nabla v$. Consequently the numerator and denominator of $m_1(.,.)$ will be balanced, and $m_1(.,.) \sim 1$. Supplementary details are given in Ref. [25].

If the anisotropic mesh is not aligned with an anisotropic function v, then similar considerations imply that the numerator and denominator of $m_1(.,.)$ are no longer balanced , and thus $m_1(.,.) \gg 1$.

In summary, the better the anisotropic mesh $\mathcal{T}_h$ is aligned with an anisotropic function v, the smaller $m_1(.,.)$ will be . This results in sharper error bounds.

3.5. Requirements on the mesh and the elements

Assumption 3.1 (*Mesh Assumptions in* Ω)**.** Let $a_1, \ldots, a_n$ be the nodes of the triangulation $\mathcal{T}_h$. In addition to the usual conformity conditions of the mesh (see [26, Chapter 2]) we demand the following assumptions.

- The number of element that contain the node a_j is bounded uniformly.
- The dimensions of adjacent element must not change rapidly, i.e.

$$h_{i,K'\sim h_{i,K}} \ \forall K, K' \text{ with } K \cap K' \neq \emptyset, i = 1, 2. \tag{19}$$

Assumption 3.2 (*General Assumptions*)**.** In our analysis, a Clément type operator I^0_{Cl} plays a vital role. Although the precise definition will be postponed until Section 4.1, we briefly describe the image space of this operator. Roughly speaking, its functions are continuous and piecewise linear for an element $K \in \mathcal{T}_h$. From now on, we use the notation

$$V^0_{\mathrm{Cl}} := \left[Im\left(I^0_{\mathrm{Cl}}\right)\right],$$

for the Clément interpolation space in Ω. The general condition is now as follows.

(H.1) The space V_h is large enough such that it contains the Clément interpolation space V^0_{Cl}, that is, $V^0_{\mathrm{Cl}} \subset V_h \cap H^1_0(\Omega)$.

(H.2) In order to obtain robust discrete solution, the elements have to be stable (i.e. the form bilinear a_h must be $\|\cdot\|_h-$coercive on V_h).

Crouzeix–Raviart Property for Nonconforming Approximation. For nonconforming approximation we require the "Crouzeix–Raviart" property:

$$(\mathrm{CR}) : \int_E [u_h]_E = 0, \forall E \in \mathcal{E}_h. \tag{20}$$

4. Analytical tools

4.1. Clément interpolation

For the analysis we require some interpolation operator that maps a function from $H_0^1(\Omega)$ to some continuous, piecewise polynomial function V_{Cl}^0. Hence Lagrange interpolation is unsuitable, but Clément like interpolation techniques have proven to be useful. The image space V_{Cl}^0 will be given by means of its basis functions. To this end denote by F_K temporarily that affine linear transformation that maps the reference element $\overline{K}$ into the actual element K. For simplicity we describe the interpolation for scalar functions.

The basis function ϕ_j associated with a node $\mathbf{x}_j$ is now uniquely determined by the condition

$$\phi_j(\mathbf{x}_i) = \delta_i^j \ \forall \mathbf{x}_i \in \mathcal{N}_h(\Omega). \tag{21}$$

Then V_{Cl}^0 is defined as the space spanned by the functions ϕ_j, for all interior nodes $\mathbf{x}_j \in \mathcal{N}_h(\Omega)$. Equivalently, it can be expressed as

$$V_{\text{Cl}}^0 := \left\{ v_h \in C^0(\Omega) : \ v_{h|K} \circ F_K \in \mathcal{P}^1(\bar{K}), \forall K \in \mathcal{T}_h \right\} \cap H_0^1(\Omega), \tag{22}$$

with $\mathcal{P}^1(\bar{K}) = \mathbb{P}^1(\bar{K})$ if K is triangle and $\mathcal{P}^1(\bar{K}) = \mathbb{Q}^1(\bar{K})$ if K is rectangle. F_K is defined as above.

Next, the Clément interpolation operator will be defined via the basis functions $\phi_j \in V_{\text{Cl}}^0$.

Definition 4.1 (*[24, Section 4] Clément Interpolation Operator*)**.** Consider an interior node $\mathbf{x}_j \in \mathcal{N}_h(\Omega)$ and the patch $w_{\mathbf{x}_j} \equiv \text{supp}(\phi_j)$, cf. Section 3.1. Define the local L^2 projection operator $P_j : L^2(w_{\mathbf{x}_j}) \longrightarrow \mathbb{P}^0(w_{\mathbf{x}_j})$ by

$$\int_{w_{\mathbf{x}_j}} (v - P_j v) w = 0 \ \forall w \in \mathbb{P}^0(w_{\mathbf{x}_j}). \tag{23}$$

Then define the Clément interpolation operator $I_{\text{Cl}}^0 : H_0^1(\Omega) \longrightarrow V_{\text{Cl}}^0 \subset H_0^1(\Omega)$ by

$$\text{I}_{\text{Cl}}^0 v := \sum_{\mathbf{x}_j \in \mathcal{N}_h(\Omega)} P_j(v)(\mathbf{x}_j)\phi_j. \tag{24}$$

We can prove the following interpolation estimates [18,24] (see also, [27,28]):

Lemma 4.1. *For all $v \in H_0^1(\Omega)$, we have:*

$$\sum_{K \in \mathcal{T}_h} h_{\min,K}^{-2} \| v - I_{\text{Cl}}^0 v \|_K^2 \lesssim m_1^2(v, \mathcal{T}_h) \| \nabla v \|_\Omega^2, \tag{25}$$

$$\sum_{E \in \mathcal{E}_h(\bar{\Omega})} \frac{h_E}{h_{\min,E}^2} \| v - I_{\text{Cl}}^0 v \|_E^2 \lesssim m_1^2(v, \mathcal{T}_h) \| \nabla v \|_\Omega^2. \tag{26}$$

4.2. Bubble functions, extension operator, inverse inequalities

For the analysis we require bubble functions and extension operators that satisfy certain properties. We start with the reference element $\overline{K}$ and define an element bubble function $b_{\overline{K}} \in C(\overline{K})$. We also require an edge bubble function $b_{\overline{E},\bar{K}} \in C(\overline{K})$ for a face $\overline{E} \subset \partial K$. Without loss of generality assume that $\overline{E}$ is on the $\bar{x}$ axis. Furthermore an extension operator $F_{\text{ext}} : C(\overline{E}) \longrightarrow C(\overline{K})$ will be necessary that acts on some function $v_{\overline{E}} \in C(\overline{E})$. Table 1 gives the definitions in each case (i.e. triangle or rectangle element).

The element bubble function b_K for the actual element K is obtained simply by the corresponding affine linear transformation. Similarly the edge/face bubble function $b_{E,K}$ is defined. Later on an edge/face bubble function b_E is needed on the domain $w_E = K_1 \cup K_2$. This is achieved by an elementwise definition, i.e.

$$b_{E|K_i} := b_{E,K_i}, i = 1, 2.$$

Analogously the extension operator is defined for functions $v_E \in C(E)$. By the same elementwise definition we obtain $F_{\text{ext}}(v_E) \in C(w_E)$. With these definitions one easily checks

$$b_K = 0 \text{ on } \partial K, \ b_E = 0 \text{ on } \partial w_E, \ \|b_K\|_\infty = \|b_E\|_\infty = 1.$$

Next, one requires the so-called inverse inequalities. They can only be expected to hold in some finite-dimensional space. The choice $\mathbb{P}^k$ covers all relevant case of our analysis.

Table 1
Bubble functions and extension operator on $\bar{K}$.

Ref. element $\bar{K}$	Bubble functions	Extention operator
 $0 \leqslant \bar{x}, \bar{y}$ $\bar{x} + \bar{y} \leqslant 1$	$b_{\bar{K}} := 3^3 \bar{x}\bar{y}(1-\bar{x}-\bar{y})$ $b_{\bar{E},\bar{K}} := 2^2 \bar{x}(1-\bar{x}-\bar{y})$	$F_{ext}(v_{\bar{E}})(\bar{x},\bar{y}) := v_{\bar{E}}(\bar{x})$
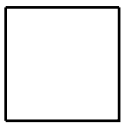 $0 \leqslant \bar{x}, \bar{y} \leqslant 1$	$b_{\bar{K}} := 2^4 \bar{x}(1-\bar{x})\bar{y}(1-\bar{y})$ $b_{\bar{E},\bar{K}} := 2^2 \bar{x}(1-\bar{x})(1-\bar{y})$	$F_{ext}(v_{\bar{E}})(\bar{x},\bar{y}) := v_{\bar{E}}(\bar{x})$

Lemma 4.2 (*Equivalences/Inverse Inequalities for Bubble Functions*). *Let $E \in \mathcal{E}(K)$ be an edge of an element K. Consider $v_K \in \mathbb{P}^{k_0}(K)$ and $v_E \in \mathbb{P}^{k_1}(E)$. Then the following equivalences/inequalities hold. The inequality constants depend on the polynomial degree k_0 or k_1 but not on K, E or v_K, v_E.*

$$\|v_K b_K^{1/2}\|_K \sim \|v_K\|_K \tag{27}$$

$$\|\nabla(v_K b_K^{1/2})\|_K \lesssim h_{\min,K}^{-1} \|v_K\|_K \tag{28}$$

$$\|v_E b_E^{1/2}\|_E \sim \|v_E\|_E \tag{29}$$

$$\|F_{ext}(v_E) b_E\|_K \lesssim h_{E,K}^{1/2} \|v_E\|_E \tag{30}$$

$$\|\nabla(F_{ext}(v_E) b_E)\|_K \lesssim h_{E,K}^{1/2} h_{\min,K}^{-1} \|v_E\|_E. \tag{31}$$

Proof. Reference [29]. □

5. Examples of finite elements

5.1. Crouzeix–Raviart elements I

For a triangulation of Ω consisting of triangles in 2D, we approximate the exact solution u in the Crouzeix–Raviart finite element space [30–32], namely,

$$V_h := \left\{ v_h \in L^2(\Omega) : \ v_{h|K} \in \mathbb{P}^1(K), \forall K \in \mathcal{T}_h, \int_E [v_h]_E = 0 \forall E \in \mathcal{E}_h \right\} \cap H_0^1(\Omega^c).$$

The bilinear form $J(.,.) : V \cup V_h \longrightarrow \mathbb{R}$ is defined here as follows:

$$J(u_h, v_h) := \sum_{E \in \mathcal{E}_h(\Omega^m)} \frac{h_E}{h_{\min,E}^2} \int_E [u_h^m]_E \cdot [v_h^m]_E, \ u_h, v_h \in V \cup V_h. \tag{32}$$

We are now able to define the norm on V_h:

$$\|v\|_h := \left(\sum_{K \in \mathcal{T}_h} |v_h^m|_{1,K}^2 + \|v_h^c\|_{1,\Omega^c}^2 + J(v_h^m, v_h^m) \right)^{1/2}. \tag{33}$$

These Crouzeix–Raviart elements are nonconforming (i.e. $V_h \not\subset V$). It is clear that the bilinear form a_h is $\|\cdot\|_h$-coercive on V_h independently of the aspect ratio of the element K of the triangulation, which means that (H.2) is valid. Since in this case we have $V_{\mathrm{Cl}}^0 = H_0^1(\Omega) \cap V_h$, the assumption (H.1) holds. In addition, the Crouzeix–Raviart elements satisfy the condition (CR) by definition.

5.2. Crouzeix–Raviart elements II

Here we restrict to a triangulation of Ω made of rectangles. Due to the condition (H.1) we actually need to modify the finite element given in [30,33]. On the reference rectangle $\bar{K} = (0, 1)^2$ we define

$$\bar{\mathbb{Q}}^{1+} := \text{span}\{1, \bar{x}, \bar{y}, \bar{x}\bar{y}, \bar{y}^2\}. \tag{34}$$

As degree of freedom (i.e. functionals of Σ) we take

$$\bar{\theta}_i(q) := \int_{\bar{E}_i} q,\ i = 1, \ldots, 4,\ \bar{\theta}_5(q) := \int_{\bar{K}} \bar{q}_5 q,$$

where $\bar{E}_i$ are the four edges of $\bar{K}$, and $\bar{q}_5$ is the polynomial defined by

$$\bar{q}_5(\bar{x}, \bar{y}) := 3(2\bar{x} - 1)(2\bar{y} - 1). \tag{35}$$

One readily checks that the triplet $\left(\bar{K}, \bar{\mathbb{Q}}^{1+}, \{\bar{\theta}_i\}_{i=1}^5\right)$ is a finite element [34, Page 75] associated basis is given by $\{\bar{q}_i\}_{i=1}^5$, where

$$\bar{q}_1(\bar{x}, \bar{y}) := 1 - 4\bar{y} + 3\bar{y}^2, \qquad \bar{q}_2(\bar{x}, \bar{y}) := -2\bar{y} + 3\bar{y}^2,$$

$$\bar{q}_3(\bar{x}, \bar{y}) := \frac{1}{2} - \bar{x} + 3\bar{y} - 3\bar{y}^2, \qquad \bar{q}_4(\bar{x}, \bar{y}) := -\frac{1}{2} + \bar{x} + 3\bar{y} - 3\bar{y}^2.$$

The edges are $\bar{E}_1 = (0, 1) \times \{0\}$, $\bar{E}_2 = (0, 1) \times \{1\}$, $\bar{E}_3 = \{0\} \times (0, 1)$ and $\bar{E}_4 = \{1\} \times (0, 1)$.

The finite element $\left(K, \mathbb{Q}^{1+}, \{\theta_i\}_{i=1}^5\right)$ on the actual anisotropic rectangle K is obtained by a standard affine transformation from $\left(\bar{K}, \bar{\mathbb{Q}}^{1+}, \{\bar{\theta}_i\}_{i=1}^5\right)$ such that $\bar{y}$ is mapped onto the stretching direction of the rectangle.

The space V_h is defined by

$$V_h := \left\{ v_h \in L^2(\Omega) :\ v_{h|K} \in \mathbb{Q}^{1+}, \forall K \in \mathcal{T}_h, \int_E [v_h]_E = 0 \forall E \in \mathcal{E}_h \right\} \cap H_0^1(\Omega^c).$$

The bilinear form $J(.,.) : V \cup V_h \longrightarrow \mathbb{R}$ is defined as in (32). The discrete norm $\|\cdot\|_h$ is also defined as in (33). The first condition (H.1) clearly holds: for rectangles, V_{Cl}^0 consists of continuous and piecewise bilinear functions. In addition, the last assumption (H.2) and the condition (CR) are satisfied trivially [18]. Note that the condition (H.1) is violated for $V_{\text{Apel}} \cap H_0^1(\Omega^c)$ (see T. Apel in [30,33]) define by

$$V_{\text{Apel}} := \left\{ v_h \in L^2(\Omega) :\ v_{h|K} \in \text{span}\{1, x, y, y^2\}\ \forall K \in \mathcal{T}_h,\ \int_E [v_h]_E = 0 \forall E \in \mathcal{E}_h \right\};$$

therefore we had to enlarge the discrete space V_h (i.e. $V_{\text{Apel}} \cap H_0^1(\Omega^c) \subset V_h$).

5.3. Crouzeix–Raviart elements III

Here we make the same restriction as in the previous section, i.e. we consider a triangulation of Ω made of rectangles. For the previous element, the local space $V_{h|K}$ depends on the stretching direction of the rectangle K. Here we modify the element such that this dependence on the directionality is removed.

Consider the reference rectangle $\bar{K} = (0, 1)^2$, set $\bar{\mathcal{P}} := \mathbb{P}^2$, and define the degrees of freedom (with the same notation as before) by

$$\bar{\theta}_i(q) := \int_{\bar{E}_i} q,\ i = 1, \ldots, 4,\ \bar{\theta}_5(q) := \int_{\bar{K}} \bar{q}_5 q,\ \bar{\theta}_6(q) := \int_{\bar{K}} q,$$

with $\bar{q}_5$ as above. One easily checks that the triplet $\left(\bar{K}, \bar{\mathcal{P}}, \{\bar{\theta}_i\}_{i=1}^6\right)$ is a finite element (cf. [34, Page 75]) whose associated basis is given by $\{\bar{q}_i\}_{i=1}^6$, with

$$\bar{q}_1(\bar{x}, \bar{y}) := 1 - 4\bar{y} + 3\bar{y}^2, \qquad \bar{q}_2(\bar{x}, \bar{y}) := -2\bar{y} + 3\bar{y}^2,$$

$$\bar{q}_3(\bar{x}, \bar{y}) := 1 - 4\bar{x} + 3\bar{x}^2, \qquad \bar{q}_4(\bar{x}, \bar{y}) := -2\bar{x} + 3\bar{x}^2.$$

$$\bar{q}_5(\bar{x}, \bar{y}) := (2\bar{x} - 1)(2\bar{y} - 1), \qquad \bar{q}_6(\bar{x}, \bar{y}) := 6(\bar{x} - \bar{x}^2 + \bar{y} - \bar{y}^2) - 1.$$

On a stretched rectangle K we take the finite element $\left(K, \mathbb{P}^2, \{\theta_i\}_{i=1}^6\right)$ obtained by a standard affine transformation from $\bar{K}$ to K, i.e. $q_i(x, y) = \bar{q}_i(\bar{x}, \bar{y})$ and $\theta_i(q) = \bar{\theta}_i(\bar{q})$. The Assumption 3.2 (i.e. (H.1) and (H.2) conditions) with the Crouzeix–Raviart condition are satisfied trivially [18], where the discrete space V_h is defined by

$$V_h := \left\{ v_h \in L^2(\Omega) :\ v_{h|K} \in \mathbb{P}^2(K), \forall K \in \mathcal{T}_h, \int_E [v_h]_E = 0 \forall E \in \mathcal{E}_h \right\} \cap H_0^1(\Omega^c),$$

and the bilinear form (resp. the discrete norm) $J(.,.)$ (resp. $\|\cdot\|_h$) are defined as above.

5.4. $\mathbb{Q}^k$ elements ($H_0^1(\Omega)$-conforme approximation)

We finally present an element currently used in *hp* finite element approximations of corner and/or edge singularities as well as boundary layers, and achieving robust exponential convergence. We consider either a 2*D* triangulation of Ω made of triangles or rectangles. The discrete space is defined for $k \geqslant 2$ by

$$V_h := \left\{ v_h \in H_0^1(\Omega) : v_h = 0 \text{ on } \partial\Omega_c,\, v_{h|K} \in \mathcal{P}_K^k, \forall K \in \mathcal{T}_h \right\} \subset V, \tag{36}$$

where $\mathcal{P}_K^k = \mathbb{Q}^k(K)$ if K is a rectangle and $\mathcal{P}_K^k = \mathbb{P}^k(K)$ if K is a triangle. The Assumption 3.2 and Crouzeix–Raviart property (CR) are clearly satisfied by definition [18].

6. Error estimators

In order to solve the coupled problem (1)–(2) by efficient adaptive finite element methods, reliable and efficient a posteriori error analysis is important to provide appropriated indicators. In this section, we first define the local and global indicators and then the lower and upper error bounds are derived.

6.1. Residual error estimator

The general philosophy of residual error estimators is to estimate an appropriate norm of the correct residual by terms that can be evaluated easier, and that involve the data at hand. To this end define the exact element residuals:

Definition 6.1 (*Exact Element Residuals*)**.** Let $v_h \in V_h$ be an arbitrary finite element function. The exact element residuals over a triangle or rectangle $K \in \mathcal{T}_h$ and over face $E \subset \overline{\Omega^c}$ are defined by

$$R_K(v_h) := f^m + \operatorname{div}(\mathbb{K}\nabla v_h^m) - \alpha_{ex}(v_h^m - v_h^c)\delta_y, \tag{37}$$

$$R_E(v_h) := f^c + \frac{d}{dx}\left(D\frac{dv_h^c}{dx}\right) + \alpha_{ex}(v_{h\,|y=0}^m - v_h^c), \tag{38}$$

respectively.

As it is common, these exact residuals are replaced by some finite-dimensional approximation called approximate element residual $r_K(v_h)$ and $r_E(v_h)$:

$$r_K(v_h) \in \mathcal{P}_K^k \text{ on } K \in \mathcal{T}_h \text{ and } r_E(v_h) \in \mathcal{P}_E^r \text{ on } E \subset \overline{\Omega^c};\, (k, r) \in \mathbb{N}^2.$$

This approximation is here achieved by projecting f^c on the space of piecewise constant functions in Ω^c and piecewise $\mathcal{P}_K^1$ functions in Ω^m for f^m, more precisely for each $E \subset \overline{\Omega^c}$, we take

$$f_E^c = \frac{1}{|E|}\int_E f^c(\tau)d\tau,$$

and for all $K \in \mathcal{T}_h$ we take f_K^m as the unique element of $\mathcal{P}_K^1$ such that

$$\int_K f_K^m(x,y)q(x,y)dxdy = \int_K f^m(x,y)q(x,y)dxdy, \forall q \in \mathcal{P}_K^1.$$

We recall that $\mathcal{P}_K^k = \mathbb{P}^k(K)$ if K is triangle, with for $E \in \mathcal{E}(K)$ $\mathcal{P}_E^r = \mathbb{P}^r(E)$. Also $\mathcal{P}_K^k = \mathbb{Q}^k(K)$ if K is rectangle, where for $E \in \mathcal{E}(K)$ $\mathcal{P}_E^r = \mathbb{Q}^r(E)$; $(k, r) \in \mathbb{N}^2$.

Thereby, we define the approximate element residuals.

Definition 6.2 (*Approximate Element Residuals*)**.** Let $v_h \in V_h$ be an arbitrary finite element function. The approximate element residuals are defined by

$$r_K(v_h) := f_K^m + \operatorname{div}(\mathbb{K}\nabla v_h^m) - \alpha_{ex}(v_h^m - v_h^c)\delta_y, \forall K \in \mathcal{T}_h, \tag{39}$$

and

$$r_E(v_h) := f_E^c + \frac{d}{dx}\left(D\frac{dv_h^c}{dx}\right) + \alpha_{ex}(v_{h\,|y=0}^m - v_h^c), \forall E \subset \overline{\Omega^c}. \tag{40}$$

We can now define the residual error estimators.

Definition 6.3 (*Residual Error Estimators*)**.** For a conforming discretization, the local residual error estimators are defined by

$$\Theta_K^2(u_h) := h_{\min,K}^2 \|r_K(u_h)\|_K^2 + \sum_{E\in\mathcal{E}_h(\partial K\cap\Omega^m)} \frac{h_{\min,K}^2}{h_E}\|[\mathbb{K}\nabla u_h^m\cdot\mathbf{n}_E]_E\|_E^2 + \sum_{E\in\mathcal{E}_h(\partial K\cap\overline{\Omega^c})} \frac{h_{\min,K}^2}{h_E}\|r_E(u_h)\|_E^2. \tag{41}$$

For a non-conforming discretization, we set,

$$\Theta_K^2(u_h) := h_{\min,K}^2 \|r_K(u_h)\|_K^2 + \sum_{E\in\mathcal{E}_h(\partial K\cap\Omega^m)} \frac{h_{\min,K}^2}{h_E}\|[\mathbb{K}\nabla u_h^m\cdot\mathbf{n}_E]_E\|_E^2 + \sum_{E\in\mathcal{E}_h(\partial K\cap\overline{\Omega^c})} \frac{h_{\min,K}^2}{h_E}\|r_E(u_h)\|_E^2 + \sum_{E\in\mathcal{E}_h(\partial K\cap\Omega^m)} \frac{h_E}{h_{\min,K}^2}\|[u_h^m]_E\|_E^2. \tag{42}$$

The global residual error estimator is given by

$$\Theta(u_h) := \left(\sum_{K\in\mathcal{T}_h}\Theta_K(u_h)^2\right)^{1/2}. \tag{43}$$

Furthermore denote the local and global approximation terms by

$$\zeta_K^2 := h_{\min,K}^2\|R_K(u_h)-r_K(u_h)\|_K^2 + \sum_{E\in\mathcal{E}_h(\partial K\cap\overline{\Omega^c})}\frac{h_{\min,K}^2}{h_E}\|R_E(u_h)-r_E(u_h)\|_E^2.$$

and

$$\zeta := \left(\sum_{K\in\mathcal{T}_h}\zeta_K^2\right)^{1/2}. \tag{44}$$

Remark 6.1. The residual character of each term on the right-hand sides of (41) and (42) is quite clear since if u_h would be the exact solution of (8), then they would vanish.

6.2. Proof of the lower error bound

To prove local efficiency for $\omega\subset\Omega$ and $v\in V\cup V_h$, let us denote by

$$\|v\|_{h,\omega}^2 := \sum_{K\subset\tilde{\omega}\cap\tilde{\Omega}^m}\|v^m\|_{1,K}^2 + \|v^c\|_{1,\tilde{\omega}\cap\tilde{\Omega}^c}^2 + \sum_{K\subset\tilde{\omega}} J_K(v^m,v^m), \tag{45}$$

where

$$J_K(v^m,v^m) := \sum_{E\in\mathcal{E}_h(\partial\Omega^m\cap\partial K)}\frac{h_E}{h_{\min,E}^2}\cdot\|[v^m]_E\|_E^2,$$

for non-conforming discretization, and we set

$$\|v\|_{h,\omega}^2 := \|v^m\|_{1,\omega\cap\tilde{\Omega}^m}^2 + \|v^c\|_{1,\omega\cap\tilde{\Omega}^c}^2, \tag{46}$$

for conforming discretization.

The error estimator $\Theta(u_h)$ is consider efficient if it satisfies the following theorem:

Theorem 6.1 (*Local Lower Error Bound*)**.** *Let $u\in V$ be the exact solution and $u_h\in V_h$ be the finite element solution. Assume that Assumption 3.1 holds. Then, the error is bounded locally from below for all $K\in\mathcal{T}_h$ by*

$$\Theta_K(u_h) \lesssim \|u-u_h\|_{h,\tilde{\omega}_K} + \sum_{K'\subset\tilde{\omega}_K}\zeta_{K'}, \tag{47}$$

where $\tilde{\omega}_K$ is a finite union of neighboring elements of K.

Proof. We begin by bounding each the residuals separately.

• **Element residual in Ω^m**: We start with the norm $\|r_K(u_h)\|_K$ of the element residual $r_K = r_K(u_h) := f_K^m + \mathrm{div}(\mathbb{K}\nabla u_h^m) - \alpha_{ex}(u_h^m - u_h^c)\delta_y$. Since we use linear or bilinear polynomial functions, $r_K \in \mathcal{P}_K^k$ holds for certain $k \in \mathbb{N}$. For $\mathbf{x} \in K$ let

$$w_K(\mathbf{x}) := r_K(u_h)(\mathbf{x}) \cdot b_K(\mathbf{x}) \in H_0^1(K), \tag{48}$$

where the element bubble function b_K is from Section 4.2. Integration by parts yields

$$\begin{aligned}
\int_K r_K \cdot w_K &= \int_K [\mathrm{div}(\mathbb{K}\nabla u_h^m) + \alpha_{ex}(u_h^m - u_h^c)\delta_y + f^m] \cdot w_K + \int_K (f_K^m - f^m) \cdot w_K \\
&= -\int_K (\mathbb{K}\nabla u_h^m) \cdot \nabla w_K + \int_K f^m \cdot w_K + \int_{K\cap\Omega^c} [\alpha_{ex}(u_h^m - u_h^c)\delta_y] \cdot w_K \\
&\quad + \int_K (f_K^m - f^m) \cdot w_K
\end{aligned}$$

We use the weak formulation (8) to obtain,

$$\begin{aligned}
\int_K r_K \cdot w_K &= \int_K [\mathbb{K}\nabla(u^m - u_h^m)] \cdot \nabla w_K \\
&\quad - \int_{K\cap\Omega^c} \alpha_{ex}[(u^m - u_h^m) - (u^c - u_h^c)]\delta_y \cdot w_K \\
&\quad + \int_K (f_K^m - f^m) \cdot w_K
\end{aligned}$$

Hence

$$\begin{aligned}
\int_K r_K \cdot w_K &\leqslant \|\mathbb{K}\nabla(u^m - u_h^m)\|_K \cdot \|\nabla w_K\|_K \\
&\quad + \alpha_{ex}\left(\|u^m - u_h^m\|_{K\cap\Omega^c} + \|u^c - u_h^c\|_{K\cap\Omega^c}\right) \cdot \|w_K\|_{K\cap\Omega^c} \\
&\quad + \|R_K(u_h) - r_K(u_h)\|_K \cdot \|w_K\|_K
\end{aligned}$$

Recalling (27), (28), and $0 \leqslant b_K \leqslant 1$ gives the following bounds,

$$\begin{aligned}
\left|\int_K r_K \cdot w_K\right| &= \|b_K^{1/2} \cdot r_K\|_K^2 \sim \|r_K\|_K^2 \\
\|\nabla w_K\|_K &= \|\nabla(b_K \cdot r_K)\|_K \lesssim h_{\min,K}^{-1} \cdot \|r_K\|_K \\
\|w_K\|_K &= \|b_K \cdot r_K\|_K \leqslant \|r_K\|_K,
\end{aligned}$$

that result in

$$h_{\min,K}^2 \cdot \|r_K\|_K^2 \lesssim \|u - u_h\|_{h,K}^2 + \zeta_K^2. \tag{49}$$

• **Normal jump in Ω^m**: Now we aim at a bound of the term $\sum_{E\in\mathcal{E}_h(\partial K\cap\Omega^m)} \frac{h_{\min,K}^2}{h_E}\|[\mathbb{K}\nabla u_h^m \cdot \mathbf{n}_E]_E\|_E^2$ of the gradient jump across some inner face $E \subset \Omega^m$. We fix $E \in \mathcal{E}_h(\Omega^m)$. Since we use linear or bilinear polynomial functions, $[\mathbb{K}\nabla u_h^m \cdot \mathbf{n}_E]_E \in \mathcal{P}_E^r$ holds for certain $r \in \mathbb{N}$. Let K_1 and K_2 be the two elements that E belongs to. The right hand side $f^m = \alpha_{ex}(u^m - u^c)\delta_y - \mathrm{div}(\mathbb{K}\nabla u^m)$ is assumed to be in $L^2(\Omega^m)$. Integration by parts yields for any function $w_E \in H_0^1(W_E)$

$$\begin{aligned}
0 &= -\int_{w_E} (\mathbb{K}\nabla u^m) \cdot \nabla w_E - \int_{w_E\cap\Omega^c} \alpha_{ex}(u^m - u^c)\delta_y \cdot w_E \\
&\quad + \int_{w_E} f^m \cdot w_E \\
-\int_E w_E \cdot [\mathbb{K}\nabla u_h^m \cdot \mathbf{n}_E]_E &= \sum_{i=1}^2 \int_{\partial K_i} w_E \cdot (\mathbb{K}\nabla u_h^m \cdot \mathbf{n}_E) \\
&= \sum_{i=1}^2 \left(\int_{K_i} \mathbb{K}\nabla u_h^m \cdot \nabla w_E + \int_{K_i} w_E \cdot \mathrm{div}(\mathbb{K}\nabla u_h^m)\right) \\
&= \sum_{i=1}^2 \left(\int_{K_i} \mathbb{K}\nabla u_h^m \cdot \nabla w_E - \int_{K_i} f_{K_i}^m \cdot w_E \right. \\
&\quad \left. + \alpha_{ex} \int_{K_i\cap\Omega^c} (u_h^m - u_h^c)\delta_y \cdot w_E\right)
\end{aligned}$$

$$= \sum_{i=1}^{2} \Big(- \int_{K_i} \mathbb{K}\nabla(u^m - u_h^m) \cdot \nabla w_E - \alpha_{ex} \int_{K_i \cap \Omega^c} [(u^m - u_h^m) - (u^c - u_h^c)]\delta_y \cdot w_E + \int_{K_i} (f^m - f_{K_i}^m) \cdot w_E \Big).$$

Let now the function $w_E \in H_0^1(w_E)$ be defined by

$$w_E := F_{ext}(-[\mathbb{K}\nabla u_h^m \cdot \mathbf{n}_E]_E) \cdot b_E, \tag{50}$$

with F_{ext} being the extension operator of Section 4.2, and b_E being the face bubble function. Because of $w_{E|E} = [\mathbb{K}\nabla u_h^m \cdot \mathbf{n}_E]_E \cdot b_{E|E}$, we conclude

$$\left\| [\mathbb{K}\nabla u_h^m \cdot \mathbf{n}_E]_E \cdot b_E^{1/2} \right\|_E^2 \lesssim \sum_{i=1}^{2} \Big\{ \left\| \mathbb{K}\nabla(u^m - u_h^m) \right\|_{K_i} \cdot \left\| \nabla w_E \right\|_{K_i} + \left(\alpha_{ex} \|u^m - u_h^m\|_{K_i \cap \Omega^c} + \|u^c - u_h^c\|_{K_i \cap \Omega^c} \right) \cdot \|w_E\|_{K_i \cap \Omega^c} + \|f^m - f_{K_i}^m\|_{K_i} \cdot \|w_E\|_{K_i} \Big\}.$$

The function w_E is piecewise cubic on $K_1 \cup K_2$. The equivalence relations (29)–(30) imply

$$\begin{aligned} \int_E w_E \cdot [\mathbb{K}\nabla u_h^m \cdot \mathbf{n}_E]_E &= \int_E [\mathbb{K}\nabla u_h^m \cdot \mathbf{n}_E]_E^2 \cdot b_E \\ &= \|[\mathbb{K}\nabla u_h^m \cdot \mathbf{n}_E]_E \cdot b_E^{1/2}\|_E^2 \\ &\sim \|[\mathbb{K}\nabla u_h^m \cdot \mathbf{n}_E]_E\|_E^2 \\ \left\| \nabla(F_{\mathrm{ext}}([\mathbb{K}\nabla u_h^m \cdot \mathbf{n}_E]_E) \cdot b_E) \right\|_{K_i} &= \|\nabla(w_E)\|_{K_i} \\ &\sim h_E^{1/2} h_{\min,K_i}^{-1} \cdot \|[\mathbb{K}\nabla u_h^m \cdot \mathbf{n}_E]_E\|_E \\ \left\| F_{\mathrm{ext}}([\mathbb{K}\nabla u_h^m \cdot \mathbf{n}_E]_E) \cdot b_E \right\|_{K_i} &= \|w_E\|_{K_i} \sim h_E^{1/2} \cdot \|[\mathbb{K}\nabla u_h^m \cdot \mathbf{n}_E]_E\|_E \end{aligned}$$

and subsequently lead to

$$\|[\mathbb{K}\nabla u_h^m \cdot \mathbf{n}_E]_E\|_E^2 \lesssim \sum_{i=1}^{2} \Big\{ \|\mathbb{K}\nabla(u^m - u_h^m)\|_{K_i} \cdot h_E^{1/2} h_{\min,K_i}^{-1} \|[\mathbb{K}\nabla u_h^m \cdot \mathbf{n}_E]_E\|_E + \left(\alpha_{ex} \|u^m - u_h^m\|_{K_i \cap \Omega^c} + \|u^c - u_h^c\|_{K_i \cap \Omega^c} \right) \cdot h_E^{1/2} \|[\mathbb{K}\nabla u_h^m \cdot \mathbf{n}_E]_E\|_E + \|f^m - f_{K_i}^m\|_{K_i} \cdot h_E^{1/2} \|[\mathbb{K}\nabla u_h^m \cdot \mathbf{n}_E]_E\|_E \Big\}.$$

The dimensions $h_E \sim h_{E,K_i}$ and $h_{\min,K_i}$ cannot change rapidly for adjacent element. Thereby,

$$\|[\mathbb{K}\nabla u_h^m \cdot \mathbf{n}_E]_E\|_E \lesssim \frac{h_E^{1/2}}{h_{\min,E}} \cdot \Big\{ \|\nabla(u^m - u_h^m)\|_{W_E} + \left(\alpha_{ex} \|u^m - u_h^m\|_{K_i \cap \Omega^c} + \|u^c - u_h^c\|_{K_i \cap \Omega^c} \right) \cdot h_{\min,E} + \|f^m - f_{K_i}^m\|_{K_i} \cdot h_{\min,E} \Big\}.$$

For a fixed element $K = K_1$ we sum up over all (inner) faces $E \in \mathcal{E}_h(\Omega^m \cap K)$ and obtain,

$$\sum_{E \in \mathcal{E}_h(\partial K \cap \Omega^m)} \frac{h_{\min,K}^2}{h_E} \|[\mathbb{K}\nabla u_h^m \cdot \mathbf{n}_E]_E\|_E^2 \lesssim \|u - u_h\|_{h,W_K}^2 + \sum_{K' \subset W_K} \zeta_{K'}^2. \tag{51}$$

• **Element residual in Ω^c**: Let $K \in \mathcal{T}_h$. Next the term $\frac{h_{\min,K}^2}{h_E} \|r_E(u_h)\|_E^2$ for a face $E \in \mathcal{E}_h(\partial K \cap \overline{\Omega^c})$ of the pipe-flow region boundary is to be bounded. Let $E \subset \overline{\Omega^c}$ and we design by K_1 and K_2 be the two elements that E belongs to (i.e. $W_E = K_1 \cup K_2$). Since we use linear or bilinear ansatz functions, $r_E = r_E(u_h) := f_E^c + \frac{d}{dx}\left(D \frac{du_h^c}{dx} \right) + \alpha_{ex}(u_{h\,|y=0}^m - u_h^c)$, $r_E \in \mathcal{P}_E^r$ holds for some $r \in \mathbb{N}$. We set:

$$w_E := (F_{\mathrm{ext}}(r_E(u_h)) \cdot b_E), \tag{52}$$

and we assume that $w_E = 0$ on $\overline{\Omega^m} \backslash \Omega^c$. We use the weak formulation (8) to obtain,

$$0 = \int_{w_E \cap \Omega^c} D \frac{du^c}{dx} \cdot \frac{dw_E}{dx} - \alpha_{ex} \int_{\Omega^c \cap W_E} (u^m - u^c) \cdot w_E - \int_{W_E} f^c \cdot w_E.$$

Integration by parts yields to

$$\begin{aligned}\int_E r_E \cdot w_E &= \int_{W_E} f_E^c \cdot w_E + \int_{W_E} \frac{d}{dx}\left(D\frac{du_h^c}{dx}\right)\cdot w_E + \alpha_{ex}\int_{W_E\cap\Omega^c}(u_h^m - u_h^c)\cdot w_E \\ &= \int_{W_E} f_E^c \cdot w_E - \int_{W_E} D\frac{du_h^c}{dx}\cdot\frac{dw_E}{dx} + \alpha_{ex}\int_{W_E\cap\Omega^c}(u_h^m - u_h^c)\cdot w_E \\ &= \int_{W_E} -(f^c - f_E^c)\cdot w_E - \int_{W_E} D\frac{d(u^c - u_h^c)}{dx}\cdot\frac{dw_E}{dx} \\ &- \alpha_{ex}\int_{W_E\cap\Omega^c}[(u^m - u_h^m) - (u^c - u_h^c)]\cdot w_E\end{aligned}$$

Because $w_{E|E} = r_E \cdot b_{E|E}$ we conclude by Cauchy–Schwarz inequality,

$$\begin{aligned}\int_E r_E^2 \cdot b_E \leqslant\ & \|f^c - f_E^c\|_{W_E}\cdot\|w_E\|_{W_E} + D\left\|\frac{d(u^c - u_h^c)}{dx}\right\|_{W_E}\cdot\left\|\frac{dw_E}{dx}\right\|_{W_E} \\ &+ \alpha_{ex}\left(\|u^m - u_h^m\|_{W_E\cap\Omega^c} + \|u^c - u_h^c\|_{W_E\cap\Omega^c}\right)\cdot\|w_E\|_{W_E\cap\Omega^c}.\end{aligned}$$

We fix $K = K_1$. Thus by inverse inequalities (29)–(31), we deduce the estimation:

$$\sum_{E\in\mathcal{E}_h(\Omega^c\cap K)}\frac{h_{\min,K}^2}{h_E}\|r_E(u_h)\|_E^2 \lesssim \|u - u_h\|_{h,W_K}^2 + \sum_{K'\subset W_K}\zeta_{K'}^2. \tag{53}$$

• **Nonconforming element:** It remains now to estimate the local indicator $\sum_{E\in\mathcal{E}_h(\partial K\cap\Omega^m)}\frac{h_E}{h_{\min,K}^2}\|[u_h^m]_E\|_E^2$. Because the jump of $u \in H_0^1(\Omega)$ is zero through all the edges of Ω, we clearly have

$$\begin{aligned}\sum_{E\in\mathcal{E}_h(\partial K\cap\Omega^m)}\frac{h_E}{h_{\min,K}^2}\|[u_h^m]_E\|_E^2 &\leqslant J_K(u_h^m, u_h^m) = J_K(u^m - u_h^m, u^m - u_h^m) \\ &\leqslant \|u^m - u_h^m\|_{h,K}^2.\end{aligned} \tag{54}$$

Summarizing, the estimates (49), (51), (53) and (54) provide the desired local lower error bound of Theorem 6.1. □

6.3. Proof of the upper error bound

The main result of this subsection can be stated as follows.

Theorem 6.2 (*Upper Error Bound-conforming Case*)**.** *Assume a conform discretization (i.e. $V_h \subset V$). Let $u \in V$ be the exact solution and $u_h \in V_h$ be the finite element solution. Assume that Assumptions 3.1 et 3.2 hold. Then the error is bounded globally from above by*

$$\|u - u_h\|_h \lesssim m_1(u - u_h, \mathcal{T}_h)\cdot\left[\Theta(u_h)^2 + \zeta^2\right]^{1/2}. \tag{55}$$

Proof. In order to derive (55) we utilize the orthogonality property of the error

$$a(u - u_h, v_h) = 0\ \forall v_h \in V_h.$$

Let $v_h \in V_h$. Integration by parts, triangle inequality and the weak formulation (8) give for all $v \in V$,

$$\begin{aligned}a(u - u_h, v) &= a(u - u_h, v - v_h) \\ &= (f^m, v^m - v_h^m)_m + (f^c, v^c - v_h^c)_c - a(u_h, v - v_h) \\ &= (f^m, v^m - v_h^m)_m + (f^c, v^c - v_h^c)_c - \int_{\Omega^m}\mathbb{K}\nabla u_h^m\cdot\nabla(v^m - v_h^m)dxdy \\ &- \int_0^L D\frac{du_h^c}{dx}\cdot\frac{d(v^c - v_h^c)}{dx}dx \\ &- \alpha_{ex}\int_0^L (u_h^m(x,0) - u_h^c(x))(v^m - v_h^m)(x,0)dx\end{aligned}$$

$$
\begin{aligned}
&+ \alpha_{ex} \int_0^L (u_h^m(x,0) - u_h^c(x))(v^c - v_h^c)(x)dx \\
&\leqslant \sum_{K\in\mathcal{T}_h} \Bigg\{ \int_K |(f^m - f_K^m)(v^m - v_h^m)| \\
&+ \int_K |r_K(u_h)(v^m - v_h^m)| + \sum_{E\in\mathcal{E}_h(K)} \int_E |[\mathbb{K}\nabla u_h^m \cdot \mathbf{n}_E]_E (v^m - v_h^m)| \\
&+ \sum_{E\in\mathcal{E}_h(K\cap\Omega^c)} \int_E |r_E(u_h)(v^c - v_h^c)| \\
&+ \sum_{E\in\mathcal{E}_h(K\cap\overline{\Omega^c})} \int_E |(f^c - f_E^c)(v^c - v_h^c)| \Bigg\} \\
&\leqslant \left(\sum_{K\in\mathcal{T}_h} h_{\min,K}^2 \|r_K(u_h)\|_K^2 \right)^{1/2} \cdot \left(\sum_{K\in\mathcal{T}_h} h_{\min,K}^{-2} \|v^m - v_h^m\|_K^2 \right)^{1/2} \\
&+ \left(\sum_{E\in\mathcal{E}_h(\Omega^m)} \frac{h_{\min,E}^2}{h_E} \|[\mathbb{K}\nabla u_h^m \cdot \mathbf{n}_E]_E\|_E^2 \right)^{1/2} \cdot \left(\sum_{E\in\mathcal{E}_h(\Omega^m)} \frac{h_E}{h_{\min,E}^2} \|v^m - v_h^m\|_E \right)^{1/2} \\
&+ \left(\sum_{E\in\mathcal{E}_h(\Omega^c)} \frac{h_{\min,E}^2}{h_E} \|r_E(u_h)\|_E^2 \right)^{1/2} \cdot \left(\sum_{E\in\mathcal{E}_h(\Omega^c)} \frac{h_E}{h_{\min,E}^2} \|v^c - v_h^c\|_E \right)^{1/2} \\
&+ \left(\sum_{K\in\mathcal{T}_h} h_{\min,K}^2 \cdot \|R_K(u_h) - r_K(u_h)\|_T^2 \right)^{1/2} \cdot \left(\sum_{K\in\mathcal{T}_h} h_{\min,K}^{-2} \|v^m - v_h^m\|_K^2 \right)^{1/2} \\
&+ \left(\sum_{E\in\mathcal{E}_h(\Omega^c)} \frac{h_{\min,E}^2}{h_E} \|R_E(u_h) - r_E(u_h)\|_E^2 \right)^{1/2} \cdot \left(\sum_{E\in\mathcal{E}_h(\Omega^c)} \frac{h_E}{h_{\min,E}^2} \|v^c - v_h^c\|_E \right)^{1/2}
\end{aligned}
$$

Every second root term is bounded by $m_1(v,\mathcal{T}_h)\cdot\|v\|_h$ by means of the interpolation Lemma 4.1. Substituting $v := u - u_h$, then the coercivity of a (i.e. $a(u-u_h, u-u_h) \gtrsim \|u-u_h\|_h^2$) yields an upper bound of the error (55). □

The upper error bound for non-conforming case on anisotropic meshes will derive as [35] in a forthcoming paper. The Section 7 gives the procedure of proving this non-conforming case. Nevertheless the upper error bound for non-conforming case on isotropic meshes is consummate in Section 7.

Commentary 6.1 (*Upper Error Bound-conforming Case*)**.** The upper error bound (55) contains an alignment measure $m_1(.,.)$. This is in contrast to estimators for isotropic meshes: For anisotropic discretizations, all known estimators are (explicitly or implicitly) based on an anisotropic mesh that is suitably aligned with the anisotropic function. Compared with the isotropic estimators, our upper error bound is special in the sense that the alignment measure cannot be evaluated explicitly. However, this should not be considered too much as a disadvantage. For example, the alignment measure $m_1(e,.)$ for the error $e = u - u_h$ is of size $\mathcal{O}(1)$ for sufficiently good meshes [24]. In practical computations one may simply use the error estimator without considering the alignment measure [24]. For adaptive algorithms this is well justified since the lower error bound (47) holds unconditionally.

6.4. Application to isotropic discretization

Since our analysis gives new results for on isotropic meshes, we here summarize them. On isotropic discretizations, our analysis holds with $h_{\min,K} \sim h_E \sim h_K$ for $E \in \mathcal{E}(K)$ and the alignment measure $m_1(.,.) \sim 1$. In other words, the above results may be rephrased as follows: the residual error estimator is here given by

$$
\Theta(u_h) := \left(\sum_{K\in\mathcal{T}_h} \Theta_K(u_h)^2 \right)^{1/2}, \tag{56}
$$

with

$$\Theta_K^2(u_h) := h_K^2 \|r_K(u_h)\|_K^2 + \sum_{E\in\mathcal{E}_h(\partial K\cap\Omega^m)} h_E \|[\mathbb{K}\nabla u_h^m \cdot \mathbf{n}_E]_E\|_E^2 + \sum_{E\in\mathcal{E}_h(\partial K\cap\overline{\Omega^c})} h_E \|r_E(u_h)\|_E^2. \tag{57}$$

for conforming discretization, and

$$\Theta_K^2(u_h) := h_K^2 \|r_K(u_h)\|_K^2 + \sum_{E\in\mathcal{E}_h(\partial K\cap\Omega^m)} h_E \|[\mathbb{K}\nabla u_h^m \cdot \mathbf{n}_E]_E\|_E^2 + \sum_{E\in\mathcal{E}_h(\partial K\cap\overline{\Omega^c})} h_E \|r_E(u_h)\|_E^2 + \sum_{E\in\mathcal{E}_h(\partial K\cap\Omega^m)} h_E \|[u_h^m]_E\|_E^2, \tag{58}$$

for non-conforming discretization. The local and global approximation terms become:

$$\zeta_K^2 := h_K^2 \|R_K(u_h) - r_K(u_h)\|_K^2 + \sum_{E\in\mathcal{E}_h(\partial K\cap\overline{\Omega^c})} h_E \|R_E(u_h) - r_E(u_h)\|_E^2.$$

and

$$\zeta := \left(\sum_{K\in\mathcal{T}_h} \zeta_K^2\right)^{1/2}. \tag{59}$$

We recall that here, h_K (resp. h_E) is the diameter of K (resp. of E). With these definitions, the lower error bound (47) of Theorem 6.1 holds for isotropic elements K. On the other hand, the upper bound (55) of Theorem 6.2 reduces to

$$\|u - u_h\|_h \lesssim \left[\Theta(u_h)^2 + \zeta^2\right]^{1/2}. \tag{60}$$

7. Concluding remarks

We have proposed and rigorously analyzed a posteriori error estimate for the finite element approximation of a coupled continuum pipe-flow/Darcy model on anisotropic meshes. This model describes flow in porous media with an embedded conduit pipe. Our investigations cover conforming and nonconforming discretizations, $2D$ domain as well as different kinds of standard elements. Much effort has been taken to impose as few assumptions as possible. For nonconforming discretizations, the main demand consists in Crouzeix–Raviart type elements. Different strategies are applied to estimate the lower and upper error bounds. These main results are summarized in Theorems 6.1 and 6.2. In order to obtain sharp bound for reliability, the anisotropic mesh has to be properly aligned, as it is the case with all known anisotropic (a posteriori) estimators. Here, this alignment enters explicitly via a so-called alignment measure. In addition, this mesh alignment is with respect to the error $e = u - u_h$. In contrast to upper error bound, the lower error bound (47) holds unconditionally. For isotropic discretizations, much of the analysis simplifies. The main results are presented in Section 6.4 and the investigations seem to be novel.

However, many issues remain to be addresses in this area:

• **Upper error bound/nonconforming case.** We give here the procedure of proving the nonconforming case for the upper error bound. To obtain the upper error bound for nonconforming case, Clément interpolation operator is not sufficient because additional term is included in the error estimator that measure the non-conformity of the method. In order to treat appropriately this non-conformity, we further need an estimate of the non-conforming error. Indeed, we can proved that (cf. [35, Lemma 4.6]),

$$\|u - u_h\|_h \lesssim m_1(u - u_h, \mathcal{T}_h) \cdot [\Theta(u_h)^2 + \zeta^2]^{1/2} + \inf_{v_h\in V\cap V_h} \|u_h - v_h\|_h. \tag{61}$$

In this estimation, $\Theta(u_h)$ is the conformity estimator of the method given by (41) and the additionally term $\inf_{v_h\in V\cap V_h} \|u_h - v_h\|_h$ measures the non-conformity of the method. If the discretization is isotropic, the non-conformity term can be bounded by using Oswald interpolation (see [36, Theorems 2.1 and 2.2]):

$$\inf_{v_h\in V\cap V_h} \|u_h - v_h\|_h \lesssim [J(u_h, u_h)]^{1/2}, \tag{62}$$

where $[J(u_h, u_h)]^{1/2}$ is the non-conformity estimator. Thus, in a forthcoming paper, we intend to proceed as in [36, Theorems 2.1 and 2.2] (see also [35, Theorem 3.3]) while building an adapted anisotropic Oswald interpolation. We present also the results of numerical tests with the finite element methods [24, Section 7].

• **CCPF model in** 3*D*. This work focuses on the 2*D*-CCPF model. In [5, Section 4], Xiaoming Wang observes that the Mathematical problem with the original CCPF and Hua's CCPF is that the fluid exchanges occur on a very singular space: point singularity in the original CCPF case and line singularity in Hua's model. He proposes the following new CCPF model assuming the simple case of an one dimensional conduit centered at the x-axis and laminar flow:

$$\left\{\begin{array}{rcll} S\frac{\partial u^m}{\partial t} - \nabla(\mathbb{K}\nabla u^m) & = & -\alpha_{ex}(u^m\delta_\Gamma - u^c\delta_\Gamma)/|\Gamma_x| + R^m & \text{in} \quad \Omega^m \\ -\frac{\partial}{\partial x}\left(D\frac{\partial u^c}{\partial x}\right) & = & \alpha_{ex}\left(\frac{1}{|\Gamma_x|}\int_{\Gamma_x} u^m dl_x - u^c\right) + R^c & \text{in} \quad \Omega^c \end{array}\right. , \tag{63}$$

where Γ is the boundary of the circular horizontal conduit centered at x-axis, Γ_x is the cross section of Γ at x (a circle), dl_x represents the infinitesimal increment of arc length on Γ_x (equivalent to $r(x)d\theta$ in the cylindrical coordinates with $r(x)$ being the radius and θ being the angle), and $|\Gamma_x|$ is the length of Γ_x which is $\pi d(x) = 2\pi r(x)$. To treat this singularity, the anisotropic meshes are more adapted (see [18]). That is why, we hope in a near further worked on this model proceeding similarly to [37, Chapter 3 and Chapter 4].

• **Boussinesq equations.** Finally, we like to extend our results to Boussinesq equations with thermocapillarity effect on the surface and nonhomogeneous boundary conditions for the velocity and the temperature [38].

Declaration of competing interest

The authors declare that they have no known competing financial interests or personal relationships that could have appeared to influence the work reported in this paper.

Acknowledgments

The author thanks African Institute for Mathematical Sciences (AIMS South Africa) for hosting him for a two months research visit. We thank Serge Nicaise (UVHC, France) for his collaboration. We would like also to thank the anonymous referees for their helpful comments that significantly improve the presentation of the paper.

References

[1] Bauer S, Liedl R, Sauter M. Modeling of karst aquifer genesis: influence of exchange flow. Water Resour Res 2003;39(10):SBH6.1–SBH6.12.
[2] Bauer S, Liedl R, Sauter M. Modeling of karst development considering conduit-matrix exchange flow. In: Sauter F, Kinzelbach W, Kovar K, Hoehn E, editors. IAHS Publ, Vol. 265. 2000, p. 10–5, Calibration and reliability in groundwater modelling: coping with uncertainty.
[3] Bauer S, Liedl R, Sauter M, Teutsch G. Hydraulic boundary conditions as a controlling factor in karst genesis. Water Resour Res 2003;39:SBH2.1–SBH2.14.
[4] Liedl R, Sauter M, Hckinghaus D, Clemens T, Teutsch G. Simulation of the development of karst aquifers using a coupled continuum pipe-flow model. Water Resour Res 2003;39:SBH6.1–SBH6.11.
[5] Wang X. On the coupled continuum pipe-flow model (CCPF) for flows in karst aquifers. Discrete Contin Dyn Syst Ser B 2010;13(2):489–501.
[6] Cao Y, Gunzburger M, Hua F, Wang X. Analysis and finite element approximation of a coupled, continuum pipe-flow/Darcy model for flow in porous media with embedded conduits. Numer Methods Partial Differential Equations 2011;27(5):1179–200.
[7] Bear J, Verruijt A. Modeling groundwater flow and pollution. Norwell, MA: D. Reidel Pub Co; 1987.
[8] Bobok E. Fluid mechanics for petroleum engineers. New York: Elsevier sci; 1993.
[9] Lei S. An analytical solution for steady state flow into a turnel. Ground Water 1999;37:23–6.
[10] Sauter M. Quantification and forecasting of regional groundwater flow and transport in a karst aquifer (Gal Lusquel Le, Malm SW Germany) (Ph.D. Thesis), Germany: Univ. of Tuingen, Tubinger; 1992.
[11] Teutsch G. Two pratical examoles from the Swabian Alb, S. Germany. In: Proceeding of 4th conference of solving groundwater problems with models. Indianapolis; 1989.
[12] Liu W, Wang Z, Li J. Anisotropic finite element approximation for a coupled continuum pipe-flow/Darcy model in karst aquifers. Comput Math Appl 2014;68:86–100.
[13] Liu W, Zhao Q, Li X, Li J. Anisotropic wilson element with conforming finite elemnt approximation for a coupled continuum pipe-flow/Darcy model in karst aquifers. Math Methods Appl Sci 2015;38:4024–37.
[14] Liu W, Kang Z, Rui H. Finite volume element approximation of the coupled continuum pipe-flow/Darcy model for flows in karst aquifers. Numer Methods Partial Differential Equations 2013;30(2).
[15] Wei L, Long X. A new nonconforming finite element with a conforming finite element approximation for a coupled continuum pipe-flow/Darcy model in karst aquifers. Numer Methods Partial Differential Equations 2016;32(3):778–98.
[16] Houédanou KW, Adetola J, Ahounou B. Residual-based a posteriori error estimates for a conforming finite element discretization of the Navier–Stokes/Darcy coupled Problem. J Pure Appl Math Adv Appl 2017;18(1):37–73.
[17] Babuška I, Rheinboldt WC. A posteriori error estimates for the finite element method. Int J Numer Methods Eng 1978;12:1597–615.
[18] Nicaise S, Creusé E. A posteriori amnestypresseerror estimation for the heteregeneous Maxwell equations on isotropic and anisotropic meshes. Calcolo 2003;40:249–71.
[19] Chen N, Gunzburger M, Huc B, Wang X, Woodruff C. Calibrating the exchange coefficient in the modified coupled continuum pipe-flow model for flows in karst aquifers. J Hydrol 2012;414:294–301.
[20] Chen Z, An K, Liu Y, Chen W. Adjoint method for an inverse problem of CCPF model. Chinese Ann Math Ser B 2014;35:337–54.
[21] Fei H. Modeling analysis and simulation of stokes-Darcy system with beavers-joseph interface condition (Ph.D. Thesis), Tallahassee: Florida State University; 2009.

[22] Wu X, Kügler P, Lu S. Identification of the exchange cofficient from indirect data for acoupled continuum pipe-flow model. Chinese Ann Math Ser B 2014;35:483–500.
[23] Kunert G. A posteriori error estimation for anisotropic tetrahedral and triangular finite element meshes. Thesis, Von der Fakultät für Mathematik der Technischen Universität chemnitz genehmigte; 1998, p. 128, amnestypresse.
[24] Creusé E, Kunert G, Nicaise S. A posteriori error estimation for the Stokes problem: Anisotropic and isotropic discretizations. Math Models Methods Appl Sci 2004;14:1297–341.
[25] Kunert G. Towards anisotropic mesh construction and error estimation in the finite element method. Numer Methods Partial Differential Equations 2002;18:625–48.
[26] Ciarlet P. The finite element method for elliptic problems. Amsterdam: North-Hollande; 1978.
[27] Houédanou KW. Analyse d'erreur a-posteriori pour quelques méthodes d'éléments finis mixtes pour le problème de transmission Stokes-Darcy : Discrétisations isotrope et anisotrope. Université d'Abomey-Calavi, thèse de Doctorat; 2015, http://hal.archives-ouvertes.fr/tel-01373344 (210 pages).
[28] Houédanou KW, Ahounou B. A posteriori error estimation for the Stokes-Darcy coupled problem on anisotropic discretization. Math Methods Appl Sci 2017;40(10):3741–74, 2016.
[29] Kunert G. An a posteriori residual error estimation for the finite element method on anisotropic tetrahedral meshes. Numer Math Springer-Verlag 2000;86:471–90.
[30] Apel T, Nicaise S, Schöberl J. A non-conforming finite element method with anisotropic mesh grading for the Stokes problem in domains with edges. IMA J Numer Anal 2001;21:843–56.
[31] Crouzeix M, Raviart PA. Conforming and non-conforming finite elments for solving the stationary Stokes equations. RAIRO Anal Numer 1973;7:33–76.
[32] Girault V, Raviart P-A. Finite element methods for navier-Stokes equations, theory and algorithms. Springer series in computational mathematics, vol. 5, Springer; 1986, amnestypresse.
[33] Apel T, Nicaise S, Schöberl J. Crouzeix-raviart type finite elements on anisotropic meshes. Numer Math 2001;89:193–223.
[34] Ern A. Aide-mémoire eléments finis. Paris: Dunod; ISBN: 2 10 007303 6, 2005.
[35] Nicaise S, Ahounou B, Houédanou W. A residual-based posteriori error estimates for a nonconforming finite element discretization of the Stokes-Darcy coupled problem: Isotropic discretization. In: Afr. Mat., Vol. 27(3). New York: African Mathematical Union and Springer-Verlag Berlin Heidelberg; 2016, p. 701–29, 2015.
[36] Karakashian O, Pascal F. A posteriori error estimates for a discontinuous Galerkin approximation of second-order problems. SIAM J Numer Anal 2003;41:2374–99.
[37] Soualem N. Estimateurs d'erreur a posteriori pour des problèmes dynamiques. Laboratoire de Mathématiques et leurs Applications de Valenciennes-FR CNRS 9556. Thèse de Doctorat; 2007, p. 139.
[38] Ahounou B, Paquet L. Existence of a variational solution for the stationary boussinesq equations with thermocapilarity effect and nonhomogenous boundary. In: Afr. Mat.. New York: African Mathematical Union and Springer-Verlag Berlin Heidelberg; 2015, http://dx.doi.org/10.1007/s13370-015-0386-6.